Solar Energy Materials & Solar Cells 103 (2012) 199–204

Contents lists available at SciVerse ScienceDirect

Solar Energy Materials & Solar Cells

journal homepage: www.elsevier.com/locate/solmat

Excess current/capacitance observation on polymer–fullerene bulk heterojunction, studied through *I–V* and *C/G–V* measurements

Pelin Kavak [a], U. Deneb Menda [a], Elif Alturk Parlak [b], Orhan Özdemir [a,*], Kubilay Kutlu [a]

[a] Yıldız Technical University, Department of Physics, Esenler-İstanbul, Turkey
[b] TUBİTAK, National Metrology Institute, Gebze-Kocaeli, Turkey

ARTICLE INFO

Article history:
Received 10 February 2012
Received in revised form
17 March 2012
Accepted 22 March 2012
Available online 25 April 2012

Keywords:
Excess current/capacitance
Conductivity modulation
Apparent building voltage
Admittance measurement

ABSTRACT

Excess current/capacitance behavior was observed on the Ag:Ca/P3HT:PCBM/PEDOT:PSS/ITO structure and the associated mechanism(s) were identified by performing both dc current–voltage (*I–V*) and ac capacitance–conductance–voltage (*C/G–V*) measurements in dark and light exposure, respectively. The excess current/capacitance issue, originated owing to a minority carrier injection, has manifested itself as conductivity modulation in *I–V* and decrease in capacitance in *C–V* at a sufficiently large forward bias. Satisfactory analysis in *I–V* as transport property and *C(G)–V* as storage feature were carried out on Ag:Ca/P3HT:PCBM/PEDOT:PSS/ITO structure.

1. Introduction

Polymer solar cells are an attractive worldwide research subject because of their low cost and ease of fabrication. Polymer solar cells made from conjugated polymers and fullerenes have a rapid progression of improvements [1–16]. Recently, new efficiency records of 7.6% was announced by Solarmer [12] on polymer/fullerene based solar cells. It has been shown that both conditions for processing of these mixtures from solution and post production treatment can have great impact on the performance of the devices, because they affect both the morphology and phase separation of the active layer [1–16].

Regioregular P3HT self-organizes into a microcrystalline structure and, because of efficient interchain transport of charge carriers, the (hole) mobility in P3HT is high (up to $\sim 0.1\ cm^2\ V^{-1}s^{-1}$) [12–16]. Moreover, in thin films interchain interactions cause a red shift of the optical absorption of P3HT, which provides an improved overlap with the solar emission. P3HT:PCBM solar cells are very sensitive to small variations in blend preparation, for example, ratio of P3HT to PCBM, solvent mixture, temperature during preparation, film thickness and annealing [12].

Using derivatives of phenylene vinylene as a hole transporting material, the device is akin to p–i–n structure in which intrinsic (undoped) film is sandwiched between two differently doped films where the p-type doped film inject holes, while electrons are supplied by the n type doped film, and recombination takes place within intrinsic layer. In this context, drift bipolar carrier transport occurs in intrinsic layer due to the applied electrical field.

Recent work on P3HT proves that it serves as efficient hole transport material while metals such as aluminum (Al) and/or silver (Ag) on P3HT (i.e., Al/P3HT and/or Ag/P3HT structure) result in the Mott–Schottky type junctions. Meanwhile, electrons could be injected as minority carriers above a certain forward bias voltage into the LUMO of the PCBM from the same electrode, and diffuse along the bulk. Consequently, P3HT HOMO serves a hole conduction band, whereas PCBM LUMO is responsible for the electron conduction band. In the mean time, ITO/PEDOT:PSS behaves as non-blocking type electrode for holes [17] at the back contact (anode). Therefore, bipolar carrier transport issue is expected for Ag:Calcium (Ca)/P3HT:PCBM/PEDOT:PSS/ITO structure, similar to p–i–n device [18].

In spite of the striking similarities in terms of carrier conductions in p–i–n devices, drastic differences are found in both current–voltage (*I–V*) and capacitance–conductance–voltage (*C/G–V*) measurements [19]. The reason behind the discrepancy between p–i–n devices and Ag:Ca/P3HT:PCBM/PEDOT:PSS/ITO structure is due to the injection of minorities that should be neutralized by holes from Ohmic side to maintain charge neutrality, leading to excess current/capacitance phenomena. In brief, injected minorities (electrons) from the cathode (Ag:Ca) should be compensated by supplying the same amount of majority carriers (holes) from anode (PEDOT:PSS/ITO) to preserve charge neutrality, thus creating the conductivity modulation issue (altering the bulk resistance of the film).

* Corresponding author. Tel.: +90 212 383 4279; fax: +90 212 383 4234.
E-mail address: ozdemir@yildiz.edu.tr (O. Özdemir).

0927-0248/$ - see front matter © 2012 Elsevier B.V. All rights reserved.
http://dx.doi.org/10.1016/j.solmat.2012.03.026

In the present work, the excess current/capacitance behavior of the Ag:Ca/P3HT:PCBM/PEDOT:PSS/ITO structure was investigated in terms of transport and storage features by performing I–V and $C(G)$–V measurements, respectively. The interpretation on conductivity modulation in I–V and decrease in capacitance in C–V at a sufficiently large forward bias were also valid for inorganic based Schottky and p–n junctions. Remarkably, satisfactory analysis in I–V as transport property and $C(G)$–V as storage feature were carried out on Ag:Ca/P3HT:PCBM/PEDOT:PSS/ITO structure.

2. Experimental

2.1. Materials and solutions

Regioregular poly(3-hexylthiophene), as a donor, [6,6]-phenyl-C_{61} butyric acid methyl ester (PCBM), as an electron acceptor were purchased from Sigma-Aldrich. Concentrations of P3HT and PCBM were 10 mg/mL, solvent was 1,2 dichlorobenzene from Sigma-Aldrich.

2.2. Film and device fabrication

The present device was fabricated on indium tin oxide (ITO) coated glass substrates with a sheet resistance 25 Ω/cm. The substrates were cleaned in an ultrasonic bath with acetone, isopropyl alcohol, and deionized-water successively for 5 min and then dried by nitrogen gas. The blended solution of P3HT:PCBM with a volume ratio of a mixture of dichlorobenzene and chloroform solvents (9:1) was prepared. PEDOT:PSS (500P) was spin-coated on the pre-cleaned ITO substrates and then heat treated for 10 min at 100 °C. Later, the blend solution was spin-coated on the PEDOT–PSS layer. The active layer was heat-treated for 10 min at 150 °C in the glove box to remove any residual solvent. Finally, the Ca/Ag cathode was vacuum evaporated and the active area was about 0.09 cm^2. The thickness of the film was determined via a mechanical profiler as 120 nm.

2.3. Measurements

The current–voltage (I–V) characteristics of device under darkness were performed by a computer-controlled current–voltage Keithley 2602A source meter at 25 °C under ambient atmosphere. For a light exposure, standard solar irradiation of 100 mW/cm^2 (AM1.5) with Xenon lamp as a light source was used to obtain I–V characteristic under illumination. In resumed conditions, an HP 4192A LCR meter operated in the frequency range $f=\omega/2\pi=400-10^6$ Hz with a 10 mV oscillation level was used to measure the admittance, Y, $(=G+j\omega C)$ from which G and C were extracted.

3. Results and discussion

3.1. Current–voltage characteristic under dark and illumination

Semilog plot of the current versus applied voltage characteristic of Ag:Ca/P3HT:PCBM/PEDOT:PSS/ITO structure is shown in Fig. 1 for both polarities under dark and illuminated conditions. As inferred from the plot, the structure possess diode behavior in dark ambience. Under light exposure, the device shows solar cell behavior. Moreover, below the built in voltage (V_{bi}), current has exponential dependence on applied bias voltage. At higher forward bias voltage, greater than V_{bi}, the voltage drop across the quasi-neutral region of the film (or bulk voltage, V_B) is non-negligible. In other words, for non-negligible V_B, forward current-forward bias voltage characteristic becomes linear, implying that the device resistance is comprised of bulk resistance and contact resistance. Although it has a poor rectifying property, the structure can be divided as depletion region with a thickness of W and the quasi-neutral bulk region of thickness $d-W$ where d is the P3HT:PCBM film thickness. Consequently, externally applied bias voltage is shared between these two regions. The voltage drop across the depletion region is junction

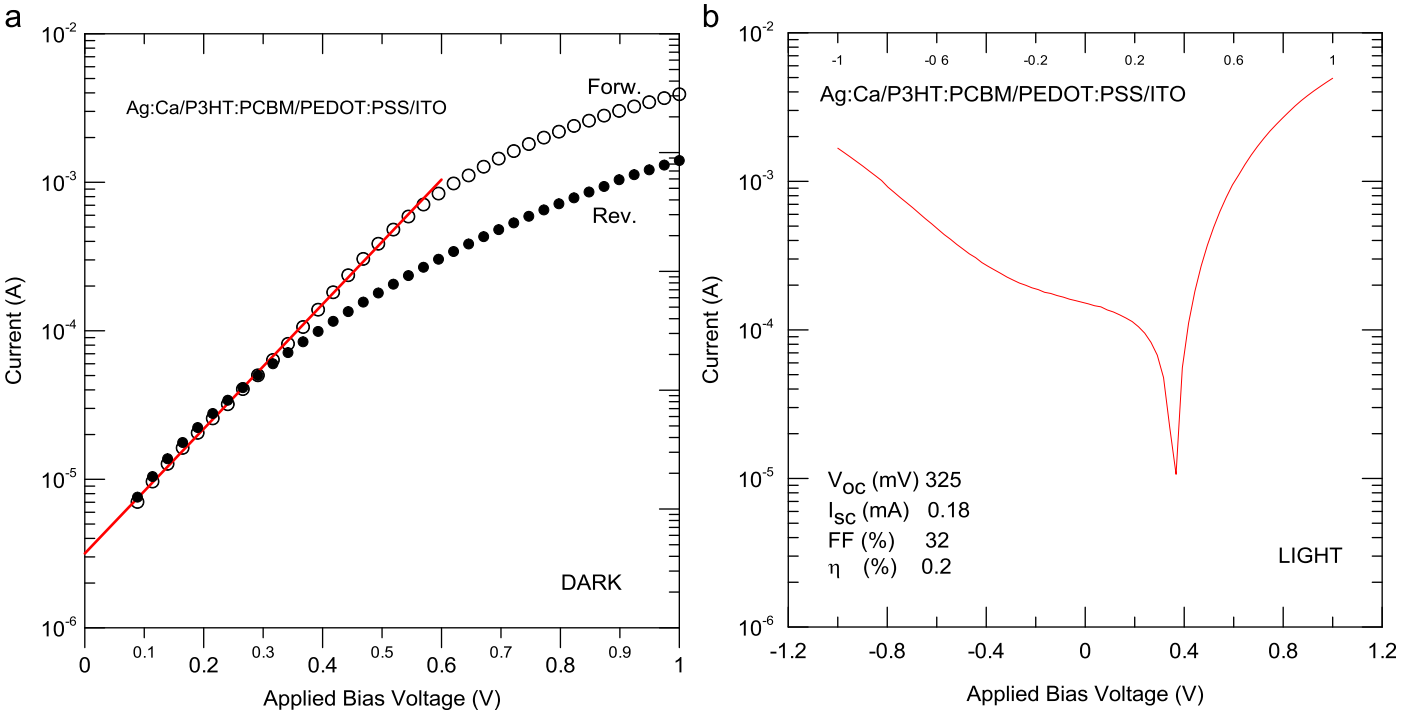

Fig. 1. (a) Room temperature dark current (I) versus applied bias voltage (V) characteristic of Ag:Ca/P3HT:PCBM/PEDOT:PSS/ITO structure under forward and reverse bias directions and (b) illuminated I/V curve and the cell parameters of Ag:Ca/P3HT:PCBM/PEDOT:PSS/ITO structure.

voltage, V_j and equals to [18,19]

$$V_j = \frac{nkT}{q} ln\left(\frac{I_F}{I_0}\right) \quad (1)$$

where n is an ideality factor, I_0 is the saturation current extrapolated at zero bias voltage, k is the Boltzmann constant, T is the temperature and q is the elementary charge. I_0 and n are extracted from the semilog plot of the I_F–V_F curve (see Fig. 1a) and determined as 3×10^{-6} A and 3.6, respectively. Therefore, V_j is calculated and its variation with externally applied bias voltage is depicted in Fig. 2(a). Moreover, V_B ($=V_F-V_j$) is also shown in the plot. As shown in the figure, the voltage drop over the bulk region is negligible at low bias values while at a larger value, it is not. Additionally, I_F versus V_B variation (given in Fig. 2b) is not linear. Both the observed non-linearity and non-obeyed power law dependence between I_F and V_B suggest the presence of an injection of minority carriers from the metal front contact (Ag:Ca) into the quasi-neutral region of P3HT:PCBM organic film. After injection, minority carriers flow away from the front contact by diffusion. However, to preserve charge neutrality of quasi-neutral region, same concentration of majority carriers (holes) should be injected from the back side of ohmic metal contact, yielding a change in the resistance of the bulk layer, in turn leading to conductivity modulation. This issue appears in I–V curves as departure from the Ohmic behavior.

The conductivity modulation issue is further approved by developing a correlation between forward bulk conductivity, σ_F, and forward current as [19]

$$\sigma_F \cong \frac{I_F(d-W)}{V_B A} \quad (2)$$

where A is the front metal contact area. Provided that W is determined from capacitance–voltage (C–V) characteristic, σ_F is obtained as a function of forward current. As depicted in Fig. 3, σ_F is constant at first at low forward bias current and denotes bulk conductivity of the film, σ_0 ($\sim10^{-7}$ Ω/cm). However, this value may not reflect the actual σ_0 due to either only bulk thickness consideration or necessity of lower frequency to determine W. From the lateral I–V characteristic of the film in planar configuration (see the inset of Fig. 3), σ_0 is measured as 10^{-8} Ω/cm [20].

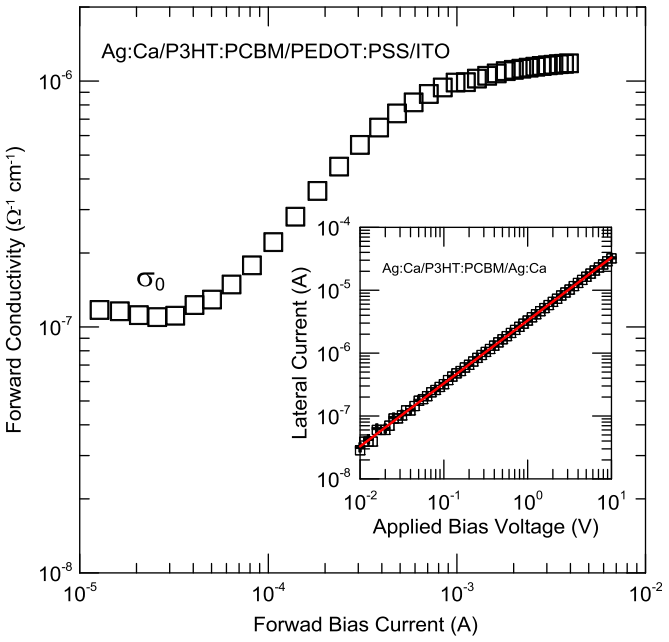

Fig. 3. Tracing of the forward conductivity as a function of forward current of Ag:Ca/P3HT:PCBM/PEDOT:PSS/ITO structure at room temperature. σ_0 denotes the unmodulated dc conductivity of the P3HT:PCBM organic film. The inset illustrates the lateral current versus applied bias voltage characteristic under planar configuration (Ag:Ca/P3HT:PCBM/Ca:Ag). Slope of this curve corresponds to bulk conductivity of P3HT:PCBM organic film.

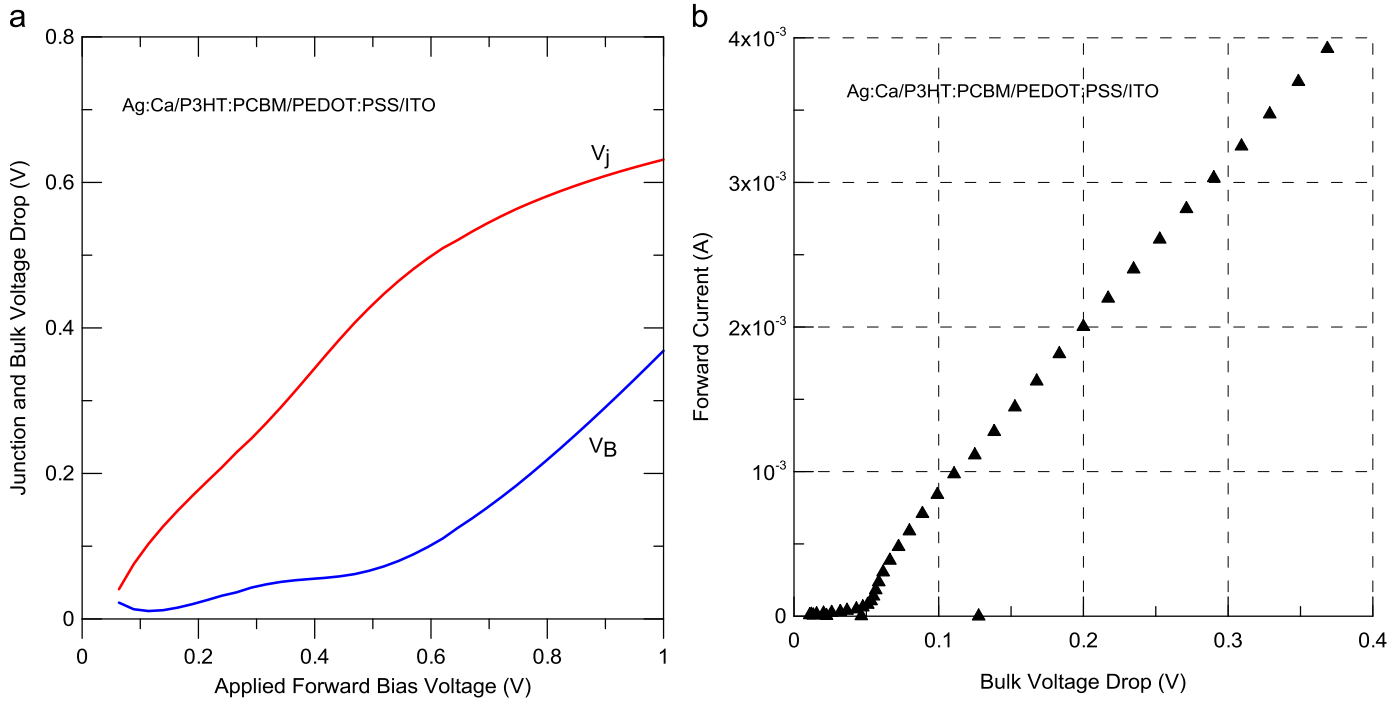

Fig. 2. (a) Junction and bulk voltage variation with applied forward bias voltage of Ag:Ca/P3HT:PCBM/PEDOT:PSS/ITO structure at room temperature under darkness. Note that the voltage drop across the bulk (V_B) is negligible at a low forward voltage so the current is barrier (junction) controlled whereas at a larger forward bias voltage, the V_B is non-negligible and device characteristic is governed by bulk limited. (b) Room temperature variation of the forward current versus bulk voltage drop. The observed nonlinearity between current and bulk voltage is indicative of conductivity modulation that is constituted by injections of minority carriers from Ag:Ca electrode and majority carriers from PEDOT:PSS/ITO to preserve the charge neutrality of P3HT:PCBM organic film.

With increasing I_F, σ_F begins to increase, deviating from σ_0. On the other side, if σ_0 is known, demarcation frequency ($f_{dem.}$) can be calculated by

$$f_{dem.} = \frac{1}{2\pi\rho\varepsilon} \tag{3}$$

with $\rho = 1/\sigma_0$ where ε is the dielectric permittivity of the film assumed as 3 [18,20–22]. Consequently, $f_{dem.}$ is calculated as 20–60 kHz [20,23,24]. Section 3.2 discusses the C–V behavior of the structure that confirms not only the value of demarcation frequency but also the expected excess capacitance issue that corresponds to conductivity modulation.

3.2. Capacitance–voltage characteristic under dark and illumination

The schematic energy band diagram of Ag:Ca/P3HT:PCBM/PEDOT:PSS/ITO structure under equilibrium, reverse/forward bias conditions and equivalent circuit are illustrated in Fig. 4. The ac parallel equivalent capacitance (C) of circuit shown in Fig. 4 is given by

$$C(\omega) = \frac{(R_j^2 C_j + R_B^2 C_B) + \omega^2 R_B^2 R_j^2 C_j C_B (C_j + C_B)}{(R_B + R_j)^2 + \omega^2 R_B^2 R_j^2 (C_j + C_B)^2} \tag{4}$$

where C_j (C_B) and R_j (R_B) are the junction (bulk) capacitance and resistance, respectively. Depending on the electrode-limited ($R_j \gg R_B$) or bulk limited ($R_j \ll R_B$) conduction type, two cases of ω ($\omega \to 0$ and $\omega \to \infty$) can be examined. In the former case (when $\omega \to 0$)

$$C(0) = \frac{(R_j^2 C_j + R_B^2 C_B)}{(R_j + R_B)^2} \tag{5}$$

If $R_j \gg R_B$ condition is held, $R_B C_B$ term becomes negligible. Then, $C(0)$ becomes,

$$C(0) = C_j = \frac{\varepsilon A}{W} \tag{6}$$

In the latter case (when $\omega \to \infty$)

$$C(\infty) = \frac{C_j C_B}{C_j + C_B} = \frac{\varepsilon A}{d} \tag{7}$$

For ω (greater than $2\pi f_{dem.}$), the states present in the film cannot follow the ac excitation and hence, the interelectrode capacitance given in relation (7) is measured. According to the C–V measurements, performed under low (below $f_{dem.}$) and high (above $f_{dem.}$) frequency, the measured capacitance would be the weighted average distance, x,

$$C = \frac{\delta Q}{\delta V} = \frac{\varepsilon A}{x} \tag{8 – a}$$

where

$$x = \frac{\int_0^\infty x \delta Q(x) dx}{\int_0^\infty \delta Q(x) dx} \tag{8 – b}$$

Generally, the Schottky junctions are majority carrier devices where ac excitation is counterbalanced by holes for p-type organic films. Consequently, the capacitance is the space charge

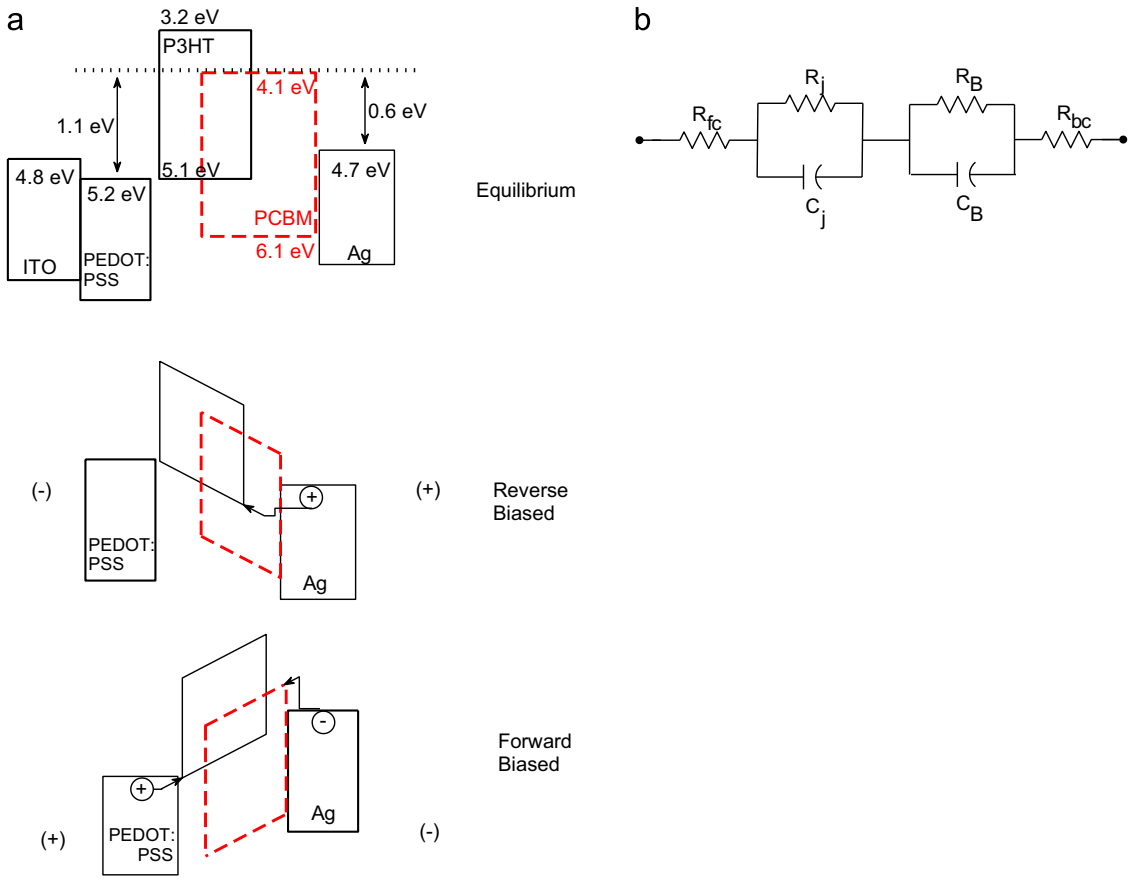

Fig. 4. (a) Hypothetical energy band diagram of Ag:Ca/P3HT:PCBM/PEDOT:PSS/ITO structure under equilibrium, reverse and forward biases conditions. Building voltage (V_{bi}), difference in work function values of PEDOT:PSS (5.2 eV) and Ag (4.7 eV), is expected around 0.5 eV. Note that hole injection from Ag under reverse bias and hole from PEDOT:PSS side and electron from Ag side under forward bias is also demonstrated. (b) Equivalent circuit diagram for Ag:Ca/P3HT:PCBM/PEDOT:PSS/ITO structure. Ag:Ca/P3HT:PCBM exhibits the Schottky barrier after the metallization (rectifying feature) and PEDOT:PSS/ITO demonstrate ohmic (non-rectifying) property. R_{fc} (R_{bc}) is due to the resistance of front (back) contact, R_j (R_B) is the junction (bulk) resistance and C_j (C_B) is the corresponding capacitance of P3HT:PCBM organic film.

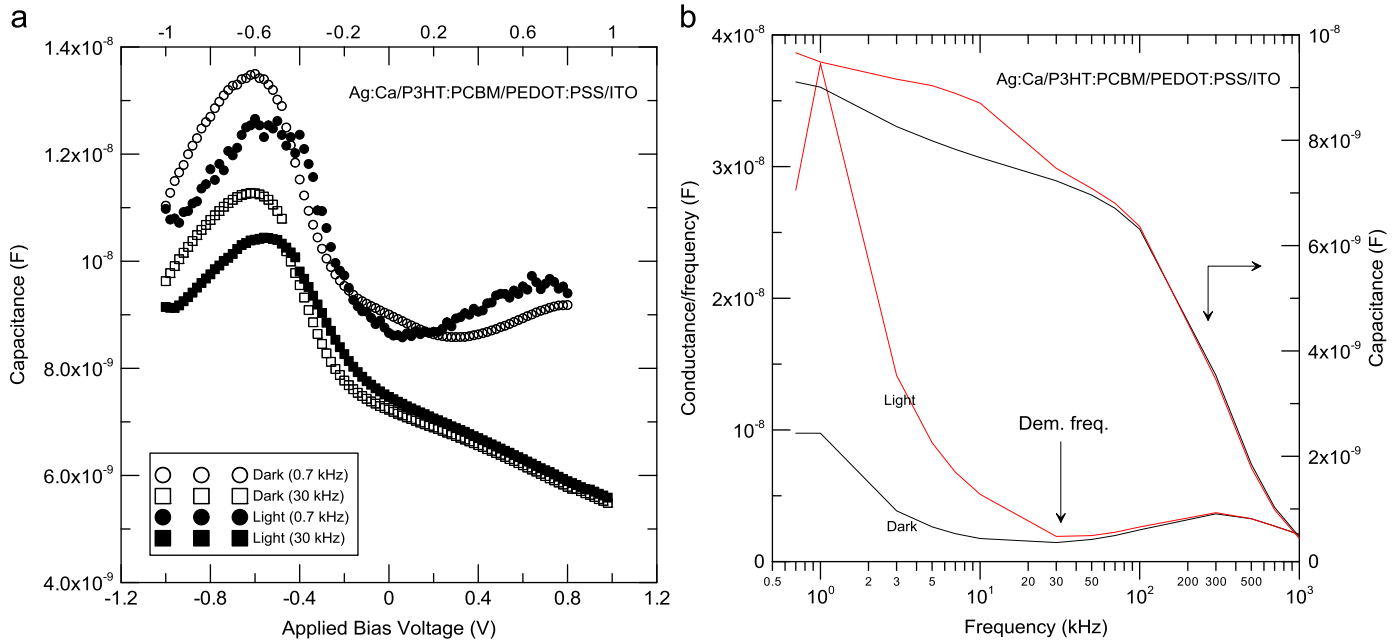

Fig. 5. (a) Room temperature capacitance versus voltage characteristic of Ag:Ca/P3HT:PCBM/PEDOT:PSS/ITO structure at selected frequencies from $400-10^6$ Hz range under dark and light conditions. The selected 700 Hz lies below the demarcation frequency ($f_{dem.}$) so-called as low frequency whereas 30 kHz display high frequency behavior. (b) Conductance and the corresponding capacitance variation as a function of scanned frequency range ($400-10^6$ Hz) at zero bias voltage. The arrow indicate the demarcation frequency($f_{dem.}$) that is consistent with the one obtained from the lateral I–V characteristic in planar configuration.

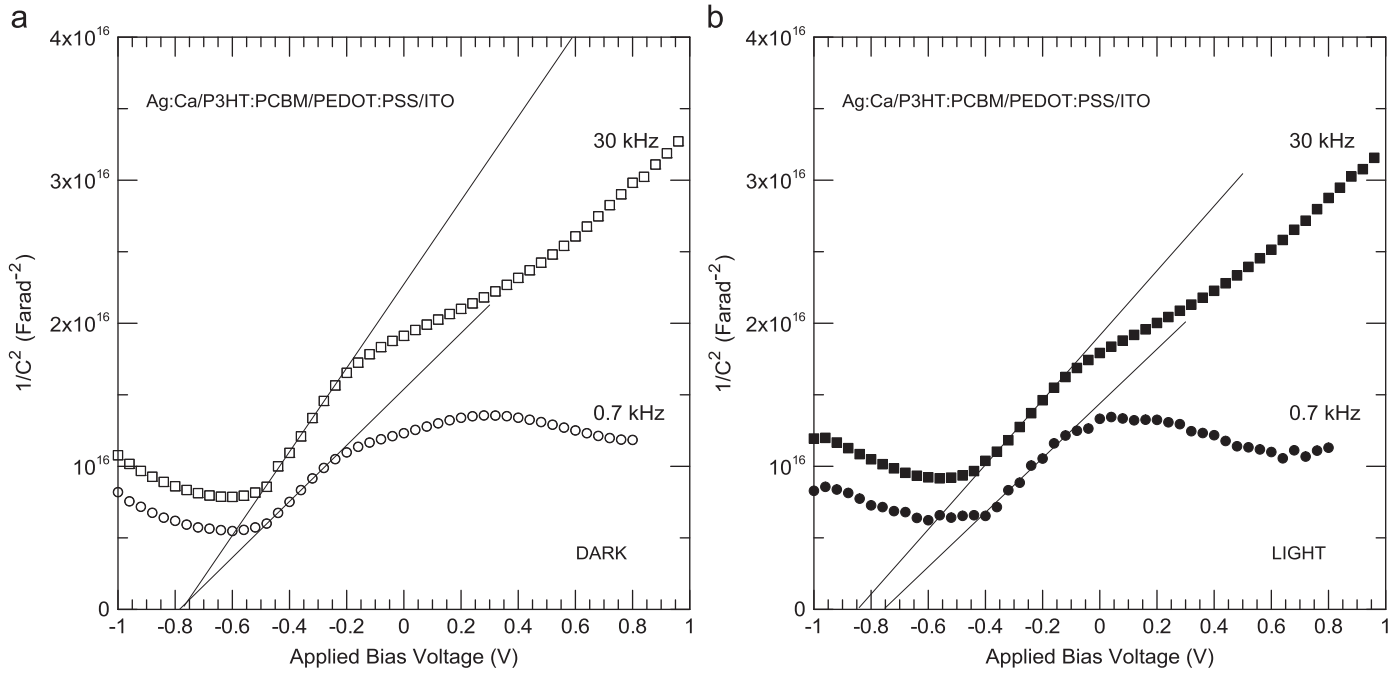

Fig. 6. Room temperature C^{-2} versus V_R curve for Ag:Ca/P3HT:PCBM/PEDOT:PSS/ITO structure at selected frequencies under (a) dark and (b) light exposure. The curve exhibits a straight line, slope of such curve yields N_I as 8.93×10^{15} cm^{-3} for 30 kHz and 2.67×10^{16} cm^{-3} for 0.7 kHz. Coinciding V_{bi} at 0.75 V exists in dark C^{-2} versus V_R curve for P3HT:PCBM by assuming $\varepsilon=3$. Under illumination, the amount of N_I increases (2.31×10^{16} cm^{-3} for 30 kHz; 2.76×10^{16} cm^{-3} at 0.7 kHz) that shifts the V_{bi}.

capacitance (depletion or junction capacitance) in the reverse and low forward bias voltages. In the case where minority carrier injection becomes non-negligible at high forward bias voltage, the situation is quite different and manifests itself in the C–V curve as the decline in capacitance beyond a peak (maximum). Obviously, this scenario is verified by the proposed equivalent circuit shown in Fig. 4. With increasing V_F, the external voltage drop on the bulk (V_B) increases (see Fig. 2a). Therefore, W becomes much smaller than $d-W$ and hence $C_B\approx0$. In other words, the bulk region is considered purely resistive. Consequently, the measured capacitance given in relation (4) becomes

$$C(\omega)=\frac{C_j}{(1+R_B/R_j)^2+\omega^2R_B^2R_j^2} \tag{9}$$

when $R_j>>R_B$, the measured capacitance begins to decline owing to the fact that C_j is shunted by the resistive divider $(1+R_B/R_j)$. As a consequence of that a new opportunity arises

for determining flat band voltage (V_{FB}) by the C–V measurement, from the corresponding bias voltage of maxima in the C–V curve.

Now, let us analyze the C–V characteristics given in Fig. 5. In the reverse and low forward bias voltages at f (30 kHz) $> f_{dem.}$ (determined from conductance variation versus f around 20 kHz, see Fig. 6b), the increase in capacitance varies from nearly interelectrode capacitance (2×10^{-9} F) towards depletion capacitance where W is calculated as 20 nm. Under such conditions, the junction capacitance is given by

$$C^{-2}=\frac{2(V_{bi}-V_R-kT/q)}{qN_I\varepsilon A^2} \tag{10}$$

where N_I is the concentration of acceptor states, whose value is determined as $8.93\times10^{15}\,cm^{-3}$ from the plot [20–24]. For $f<f_{dem.}$, N_I is obtained as $3.67\times10^{16}\,cm^{-3}$ and the difference is interpreted as due to the states that are able to follow the ac excitation and dc bias variation. The extrapolation of C^{-2} versus V curve (at $C^{-2}=0$) provides the built-in voltage. As shown in Fig. 6(a), it is determined as 0.75 V. It should kept in mind that because of the presence of minority carrier build up layer (inversion layer) at the interface, the obtained V_{bi} is not actual. Rather it is apparent and greater than the expected value, ($\sim$0.5 eV) which is the difference of work function of PEDOT:PSS (5.2 eV) and Ag (4.7 eV) [24,25]. However, the barrier height for Ag is determined as 0.44 eV from the lateral I–V curve of the film in planar configuration and it seems plausible.

The measurement is repeated under 100 mW/cm^2 light exposure. At low frequency, the bulk capacitance is short-circuited and hence measured capacitance is defined only by junction capacitance, C_j. The variation of C_j with applied reverse bias voltage is due to the depletion layer width, given by

$$W=\left[\frac{2\varepsilon(V_{bi}-V_R)}{qN_I}\right]^{1/2} \tag{11}$$

At high frequency, on the other hand, the capacitance decreases steadily towards geometrical or interelectrode capacitance, 2×10^{-9} F. At large forward bias where minority carrier injection is non-negligible, the drift and diffusion processes of minorities (electrons) interact and provide inductive (L) contribution in which capacitance becomes negative and would be

$$C=(\omega^2L)^{-1} \tag{12}$$

This issue is related to the change of R_B due to hole injection, called as conductivity modulation in the previous I–V part. The rate of its change under injection demands time so delay takes place with respect to the applied bias voltage. The inductive effect can be eliminated at high frequency greater than $f_{dem.}$. Apparently, its contribution is influenced due to deep recombination centers at the edge of junction region. Indeed, the similar suggestions are proposed in other works [17,18].

As a final remark, the corresponding bias (0.6 V) at the onset of capacitance decline and the hypothetically displayed energy band diagram, given in Fig. 4, coincide with each other. Moreover, illumination increases the amount of previously build-up minorities and hence shifts the apparent V_{bi} [18].

4. Conclusion

Minority carrier injection at a large forward bias was responsible for the excess current/capacitance phenomenon in the present bulk heterojunction in dc current–voltage and ac capacitance–conductance–voltage measurements. The energy band diagram and its equivalent circuits resolved the issue adequately. Finally, building up the minorities caused an apparent built-in voltage in the present junction.

Acknowledgment

This work was carried out with the financial support of Yıldız Technical University Project: 2011-01-01-KAP03. The authors are grateful to Prof. Dr. Yani Skarlatos for careful reading.

References

[1] C.J. Brabec, N.S. Sariciftci, J.C. Hummelen, Plastic solar cells, Advanced Functional Materials 11 (2001) 15–26.
[2] H. Spanggaard, F.C. Krebs, A brief history of the development of organic and polymeric photovoltaics, Solar Energy Materials and Solar Cells 83 (2004) 125–146.
[3] K.M. Coakley, M.D. McGehee, Conjugated polymer photovoltaic cells, Chemistry of Materials 16 (2004) 4533–4542.
[4] H. Hoppe, N.S. Sariciftci, Organic solar cells: an overview, Journal of Materials Research 19 (2004) 1924–1945.
[5] S. Gunes, H. Neugebauer, N.S. Sariciftci, Conjugated polymer based organic solar cells, Chemical Reviews 107 (2007) 1324–1338.
[6] C. Winder, N.S. Sariciftci, Low bandgap polymers for photon harvesting in bulk heterojunction solar cells, Journal of Materials Chemistry 14 (2004) 1077–1086.
[7] F.C. Krebs (Ed.), The development of organic and polymer photovoltaics, Solar Energy Materials and Solar Cells 83 (2004) 125–322.
[8] S.E. Shaheen, D.S. Ginley, G.E. Jabbour (Eds.), Organic-Based Photovoltaics, MRS Bulletin 30 (2005) 10–19 .
[9] F.C. Krebs (Ed.), Low band gap polymer materials for organic photovoltaics, Solar Energy Materials and Solar Cells 91 (2007) 954–985.
[10] M.T. Loyd, J.E. Anthony, C.G. Malliaras (Eds.), A real alternative. Materials and devices for cheap efficient solar power, Materials Today 10 (2007) 28–33.
[11] C.J. Brabec, N.S. Sarıciftci, F. Padingnger, T. Fromherz, J.C. Hummelen, 2.5% efficient organic plastic solar cells, Physics Letters 78 (2001) 841–843.
[12] 〈http://www.pv-tech.org/news〉.
[13] T.J. Prosa, M.J. Winokur, J. Moulton, P. Smith, A.J. Heeger, X-ray structural studies of poly(3-alkylthiophenes): an example of an inverse comb, Macromolecules 25 (1992) 4364–4372.
[14] Z. Bao, A. Dodabalapur, A. Lovinger, Soluble and processable poly3-hexylthophene, Applied Physics Letters 69 (1996) 4108–4110.
[15] H. Sirringhaus, P.J. Brown, R.H. Friend, M.M. Nielsen, K. Bechgaard, B.M.W. Langeveld-Voss, A.J.H. Spiering, R.A.J. Janssen, E.W. Meijer, P. Herwig, D.M. de Leeuw, Two-dimensional charge transport in self-organized, high-mobility conjugated polymers, Nature 401 (1999) 685–688.
[16] W. Ma, C. Yang, K. Lee, A.J. Heeger, Thermally stable, efficient polymer solar cells with nanoscale control of interpenetrating network morphology, Advanced Functional Materials 15 (2005) 1517–1522.
[17] P.B. Boix, J. Ajuria, I. Etxebarria, R. Pacios, G. Garcia-Belmonte, Kinetics of occupancy of defect states in poly (3-hexylthiophene):fullerene solar cells, Thin Solid Films, doi:10.1016/j.tsf.2011.09.044.
[18] G. Garcia-Belmonte, A. Munar, E.M. Barea, J. Bisquert, I. Ugarte, R. Pacios, Charge carrier mobility and lifetime of organic bulk heterojunctions analyzed by impedance spectroscopy, Organic Electronics 9 (2008) 847–851.
[19] J. Kanicki (ed.), Amorphous and Microcrystalline Semiconductor Devices, Volume II. Materials and Device Physics, Artech House Boston, 1982, pp. 189–279.
[20] J.V. Li, A.M. Nardes, Z. Liang, S.E. Shaheen, B.A. Gregg, D.H. Levi, Simultaneous measurement of carrier density and mobility of organic semiconductors using capacitance techniques, Organic Electronics 12 (2011) 1879–1885.
[21] C. Lungenschmied, E. Ehrenfreund, N.S. Sarıcifci, Negative capacitance and its photo-inhibition in organic bulk heterojunction devices, Organic Electronics 10 (2009) 115–119.
[22] C.-M. Kang, S. Kim, Y. Hong, C. Lee, Frequency analysis on poly(3-hexylthiopene) rectifier using impedance spectroscopy, Thin Solid Films 518 (2009) 889–892.
[23] I.S. Yahia, H.S. Hafez, F. Yakuphanoglu, B.F. Senkal, M.S.A. Abdel Mottaleb, Photovoltaic and impedance spectroscopy analysis of p–n like junction for dye sensitized solar cell, Synthetic Metals 161 (2011) 1299–1305.
[24] A. Seeman, T. Sauermann, C. Lungenschmied, O. Armbruster, S. Bauer, H.-J. Egelhaaf, J. Hauch, Reversible and irreversible degradation of organic solar cell performance by oxygen, Solar Energy 85 (2011) 1238–1249.
[25] C.-Y. Nam, D. Su, C.T. Black, High performance air-processed polymer–fullerene bulk heterojunction solar cells, Advanced Functional Materials 19 (2009) 1–8.